AGU PUBLICATIONS

Earth's Future

RESEARCH ARTICLE
10.1002/2014EF000265

Remote sensing of fugitive methane emissions from oil and gas production in North American tight geologic formations

Oliver Schneising[1], John P. Burrows[1,2,3], Russell R. Dickerson[2], Michael Buchwitz[1], Maximilian Reuter[1], and Heinrich Bovensmann[1]

[1]Institute of Environmental Physics (IUP), University of Bremen, Bremen, Germany, [2]Department of Atmospheric and Oceanic Science, University of Maryland, College Park, Maryland, USA, [3]NERC Centre for Ecology and Hydrology, Wallingford, UK

Key Points:
- Emissions of oil and gas industries are constrained using satellite observations
- Current inventories likely underestimate fugitive methane emissions
- Climate benefit of transition to unconventional oil and gas is questionable

Corresponding author:
O. Schneising, oliver.schneising@iup.physik.uni-bremen.de

Citation:
Schneising, O., J. P. Burrows, R. R. Dickerson, M. Buchwitz, M. Reuter, and H. Bovensmann (2014), Remote sensing of fugitive methane emissions from oil and gas production in North American tight geologic formations, *Earth's Future*, *2*, doi:10.1002/2014EF000265.

Received 3 JUL 2014
Accepted 28 AUG 2014
Accepted article online 4 SEP 2014

Abstract In the past decade, there has been a massive growth in the horizontal drilling and hydraulic fracturing of shale gas and tight oil reservoirs to exploit formerly inaccessible or unprofitable energy resources in rock formations with low permeability. In North America, these unconventional domestic sources of natural gas and oil provide an opportunity to achieve energy self-sufficiency and to reduce greenhouse gas emissions when displacing coal as a source of energy in power plants. However, fugitive methane emissions in the production process may counter the benefit over coal with respect to climate change and therefore need to be well quantified. Here we demonstrate that positive methane anomalies associated with the oil and gas industries can be detected from space and that corresponding regional emissions can be constrained using satellite observations. On the basis of a mass-balance approach, we estimate that methane emissions for two of the fastest growing production regions in the United States, the Bakken and Eagle Ford formations, have increased by 990 ± 650 ktCH$_4$ yr^{-1} and 530 ± 330 ktCH$_4$ yr^{-1} between the periods 2006–2008 and 2009–2011. Relative to the respective increases in oil and gas production, these emission estimates correspond to leakages of $10.1\% \pm 7.3\%$ and $9.1\% \pm 6.2\%$ in terms of energy content, calling immediate climate benefit into question and indicating that current inventories likely underestimate the fugitive emissions from Bakken and Eagle Ford.

1. Introduction

Horizontal drilling and hydraulic fracturing, which enable to tap tight rock formations, are a significant component of the recent increases in Northern American gas and oil production. Besides their inherent economic advantages, these unconventional energy resources represent potentially an opportunity to reduce greenhouse gas emissions because the combustion of natural gas or oil produces less CO_2 per unit of energy than that of coal (about 56% for gas and 79% for oil) [*U.S. Energy Information Administration*, 2011]. However, the climate benefit from shifting away from coal is offset by fugitive methane release during the fracturing, production, and distribution process [*Howarth et al*., 2011; *Alvarez et al*., 2012; *Brandt et al*., 2014; *Jackson et al*., 2014]. This is because methane is the second most important anthropogenic greenhouse gas, being 34 times more potent per unit of mass than CO_2 when including carbon-climate feedbacks and considering a time horizon of 100 years [*Intergovernmental Panel on Climate Change*, 2013].

In contrast to conventional gas and oil production, a significant amount of methane is already emitted during well completion [*Howarth et al*., 2011]. This occurs when the fracturing fluid, which is injected into the dense nonporous medium at high pressures to create fissures allowing migration of the imbedded resources, flows back, and when the plugs that separated the sections of the fracturing stages of the well are drilled out. In the production process of tight oil, co-occurring natural gas is typically used to drive the oil to the wellbore [*U.S. Energy Information Administration*, 2013].

As the productivity of these unconventional wells is initially high but depletes rapidly, new wells are continuously being drilled. Therefore, methane emissions from field production of oil and gas from tight reservoirs have the potential to reverse the climate impact mitigation, at least in the short run, if the leakage rate exceeds the break-even point. In this context, it has been estimated that a net climate benefit of switching from coal-fired to gas-fired power plants can only be achieved on all time frames, if natural gas leakage in the full system from well to delivery is less than 3.2% [*Alvarez et al*., 2012].

Assessing the climate implications of the gas and oil production from tight reservoirs is difficult due to the lack of reliable emission estimates. The latest estimate of methane emissions from natural gas systems reported by the U.S. Environmental Protection Agency (EPA) is 6343 kt in 2011, corresponding to 1.2% of the gross U.S. natural gas production (0.9%–1.7% at the 95% confidence level) [*U.S. Environmental Protection Agency*, 2014], while previous reports assumed 1.4% (1.0%–1.8%) [*U.S. Environmental Protection Agency*, 2013] and 2.0% (1.5%–2.7%) [*U.S. Environmental Protection Agency*, 2012]. Such revisions indicate that the uncertainties of these bottom-up estimates are larger than suggested by the reported small uncertainty ranges. EPA's equivalent estimate of methane released to the atmosphere by petroleum systems corresponds to 0.7% of the U.S. crude oil production (0.5%–1.7% at the 95% confidence level) [*U.S. Environmental Protection Agency*, 2012, 2013, 2014].

The recent downscaling of estimated bottom-up emissions is in line with the direct measurements of methane emissions sampled at selected onshore natural gas sites throughout the United States (May to December 2012) provided by the participating utility companies [*Allen et al.,* 2013]. The corresponding bottom-up estimate of the methane leakage rate is based on summing emissions from different types of known sources and is slightly lower than the EPA estimate. However, several top-down estimates based on measurements of ambient methane provide evidence for considerably larger emissions [*Pétron et al*., 2012; *Karion et al*., 2013; *Miller et al*., 2013; *Caulton et al*., 2014]: a recent study based on tall tower flask samples and aircraft profiles concludes that anthropogenic methane emissions in the United States might be 50% higher than inventory estimates with even larger discrepancies over the gas and oil production areas in the south-central states Texas, Oklahoma, and Kansas [*Miller et al*., 2013]. Methane emissions from the Denver-Julesburg Basin (Colorado) are also likely underestimated in current inventories, as is concluded from tall tower samples (2007–2010) and road surveys (June to July 2008) [*Pétron et al*., 2012]. An estimate of methane fluxes of the Uintah Basin (Utah) using aircraft measurements (February 2012) provides exceedingly large leakage rates negating any short-term climate benefit of tight resources from this basin [*Karion et al*., 2013]. These studies are also part of a systematic comparison of published CH_4 emission estimates with inventory data, which concludes that emissions from U.S. and Canadian natural gas systems appear larger than official estimates [*Brandt et al*., 2014]. This is also supported by another very recent analysis, finding the possibility of a large fugitive methane emission rate over the Marcellus shale formation (Pennsylvania) using an instrumented aircraft platform (June 2012) [*Caulton et al*., 2014]. Methane emissions from tight oil production are less well investigated so far and thus even more uncertain.

To better understand to what extent the discrepancies between these bottom-up and top-down estimates are caused by regional emission differences, e.g., due to different regulations, standards, and practices, it is essential to derive further emission estimates for other formations, in particular those including hitherto understudied tight oil production. In this manuscript, we present an analysis of column-averaged dry air mole fractions of atmospheric methane (denoted XCH_4) retrieved from the SCIAMACHY (SCanning Imaging Absorption spectroMeter for Atmospheric CHartographY) satellite instrument to quantify methane emissions from the Bakken and Eagle Ford formations, the fastest growing oil production regions in the United States [*U.S. Energy Information Administration*, 2014a]. Furthermore, we also find methane enhancements over the Marcellus formation, which is the largest source of natural gas in the United States and exhibits incessant production growth [*U.S. Energy Information Administration*, 2014a]. This study complements previous measurement-based emission estimates in other regions, which were largely obtained during short-duration campaigns. The results suggest that methane emissions from the two not-yet-studied source regions, Bakken and Eagle Ford, are also underestimated in current bottom-up inventories.

2. Data Set

We analyzed XCH_4 retrieved from SCIAMACHY onboard the ENVISAT satellite (launched in 2002, end of mission declared in 2012) [*Burrows et al*., 1995; *Bovensmann et al*., 1999] using the latest version (v3.7) of the Weighting Function Modified DOAS (WFM-DOAS) algorithm [*Schneising et al*., 2011, 2012]. ENVISAT was launched into a sun-synchronous orbit with an equator crossing time of 10:00 A.M. local time and a repeat cycle of 35 days. The horizontal resolution of the SCIAMACHY nadir measurements, which depends

on orbital position and spectral interval, is typically 60 km across track by 30 km along track for the spectral fitting windows used in this study. As a result of the observation of reflected solar radiation in the near-infrared/shortwave infrared (NIR/SWIR) spectral range, SCIAMACHY yields atmospheric methane with high sensitivity in the planetary boundary layer (Figure 1) and is thus well suited to study emissions from oil and gas fields.

The 1024 pixel detector array of the relevant SCIAMACHY NIR/SWIR channel 6 uses two different compositions of InGaAs as detector material. The lower wavelength part (970–1590 nm) consists of lattice-matched InGaAs, exhibiting perfect match between the lattice constants of the detector material and the InP substrate. The extended-wavelength part (1590–1770 nm), covering the methane $2\nu_3$ absorption band around 1666 nm used for the methane retrieval, is doped with higher amounts of indium to tune the bandgap to be sensitive to longer wavelengths. The associated strain within the material makes these extended-wavelength detector pixels subject to irreversible displacement damage induced by high-energy solar protons, which occurs from time to time at individual detector pixels and is identified by SCIAMACHY's in-flight calibration measurements [*Kleipool et al*., 2007]. Therefore, different strict static detector pixel masks, excluding affected pixels, are used in the retrieval for different time periods. Each mask is optimized for the respective end of the period to ensure stability during the whole time interval. The retrieval results since November 2005 are all based on the same detector pixel mask assuring consistent retrievals throughout the entire period relevant for the presented analysis (2006–2011). As a consequence of the effective reduction of detector pixels and corresponding lowering of the signal-to-noise of methane absorption, the single measurement precision changes from about 30 ppb before November 2005 to about 70 ppb afterward [*Schneising et al*., 2011]. Based on a validation with ground-based Fourier Transform Spectrometer measurements of the Total Carbon Column Observing Network [*Wunch et al*., 2011], which focuses on the period since November 2005, the relative accuracy of the SCIAMACHY data set is estimated to be about 8 ppb [*Dils et al*., 2014].

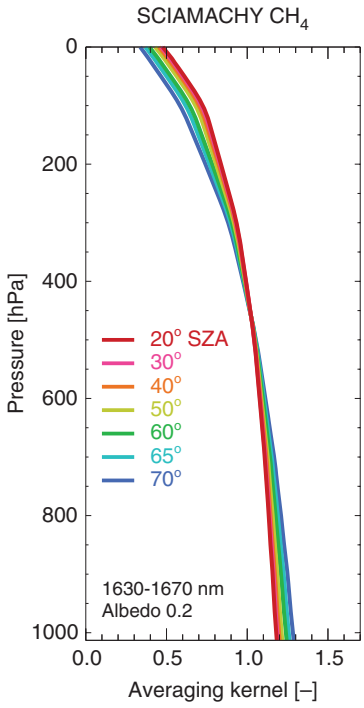

Figure 1. Averaging kernels reflecting the altitude sensitivity of the retrievals.

Figure 2 gives an overview of the long-term global XCH_4 data set showing column-averaged dry air mole fractions as a function of latitude and time. The interhemispheric gradient and the seasonal cycle, as well as the renewed methane growth since about 2007 [*Rigby et al*., 2008; *Dlugokencky et al*., 2009], are all clearly detected. The origins of the recent methane growth are not completely understood, but the growth of anthropogenic emissions, such as massive hydraulic fracturing, may play a role [*Bergamaschi et al*., 2013; *Nisbet et al*., 2014].

3. Methods

Averaged XCH_4 over the United States for the periods 2006–2008 and 2009–2011 is shown in Figure 3, in which the target regions containing the formations discussed in this manuscript are highlighted. As the relatively small methane enhancements owing to fugitive methane emissions in the oil and gas production process are superimposed by other larger signals, the following approach is used to extract these typically not immediately obvious increases from the data.

For the selected target regions, we compute anomalies in XCH_4 by subtracting the monthly mean values of the satellite XCH_4 for the respective entire region from the individual measurements. This filters out large-scale seasonal variations or global increase yielding regional enhancements relative to varying background concentrations [*Schneising et al*., 2013].

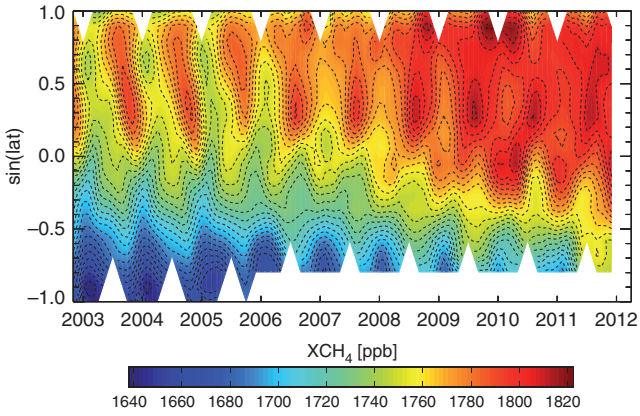

Figure 2. Overview of the long-term global satellite XCH_4 data set derived from SCIAMACHY; shown are column-averaged dry air mole fractions of methane as a function of latitude and time.

The lower retrieval precision since the end of 2005 requires that many measurements need to be averaged to achieve the signal-to-noise to identify the fugitive methane emissions, which are expected to result in enhancements of the column-averaged mole fractions in the order of a few ppb. Therefore, the satellite anomalies are averaged over the time periods 2006–2008 and 2009–2011, between which oil and gas production in Bakken, Eagle Ford, and Marcellus grew significantly [*U.S. Energy Information Administration*, 2014a]. The differences of these two periods are shown in Figures 4 and 5 (gridded 0.5° × 0.5°, effective resolution ~2° × 2° after smoothing) highlighting the changes in atmospheric methane abundance between both periods. In terms of interperiod variability, this approach separates regional emission trends from in first-order approximation temporally constant other intraregional emission signals or a wide range of potentially remaining systematic retrieval biases. Accordingly, the local increases from growing oil and gas exploitation in specific tight formations can be teased out of the data.

The boundary layer mean of zonal and meridional winds, u and v, as provided by the ERA-Interim reanalysis product [*Dee et al*., 2011] of the European Centre for Medium-Range Weather Forecasts (ECMWF), is first computed for every single measurement individually. The boundary layer height is determined from the potential temperature [*Draxler and Hess*, 2010]. The absolute values of wind components are then gridded and temporally averaged in exactly the same manner as the methane data resulting in mean values $\overline{u}$ and $\overline{v}$ for the entire hot spot area.

To quantify the emission change, we used a simple model with a box B placed over the source region (shown in red in Figure 4). The absolute average mass flux F per unit of time inside the box was computed from the net enhancements perpendicular to the meridional and zonal direction relative to the respective background E_m, E_z (in units of mass per area), and average horizontal boundary layer wind,

$$F = \frac{\overline{u}^2 E_m l_m + \overline{v}^2 E_z l_z}{\sqrt{\overline{u}^2 + \overline{v}^2}} = \frac{\overline{u}^2 \Delta l_m \sum_{i=1}^{n_m} E_{m,i} + \overline{v}^2 \Delta l_z \sum_{j=1}^{n_z} E_{z,j}}{\sqrt{\overline{u}^2 + \overline{v}^2}} \quad , \tag{1}$$

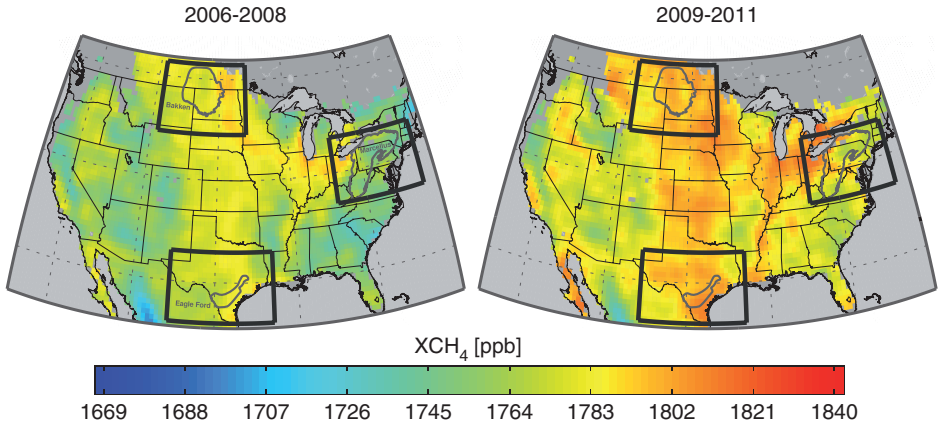

Figure 3. XCH_4 over the United States for the two periods 2006–2008 and 2009–2011. Shown are those gridcells, which contain more than 65 measurements in both periods. The target regions which are studied in more detail are highlighted by the three boxes.

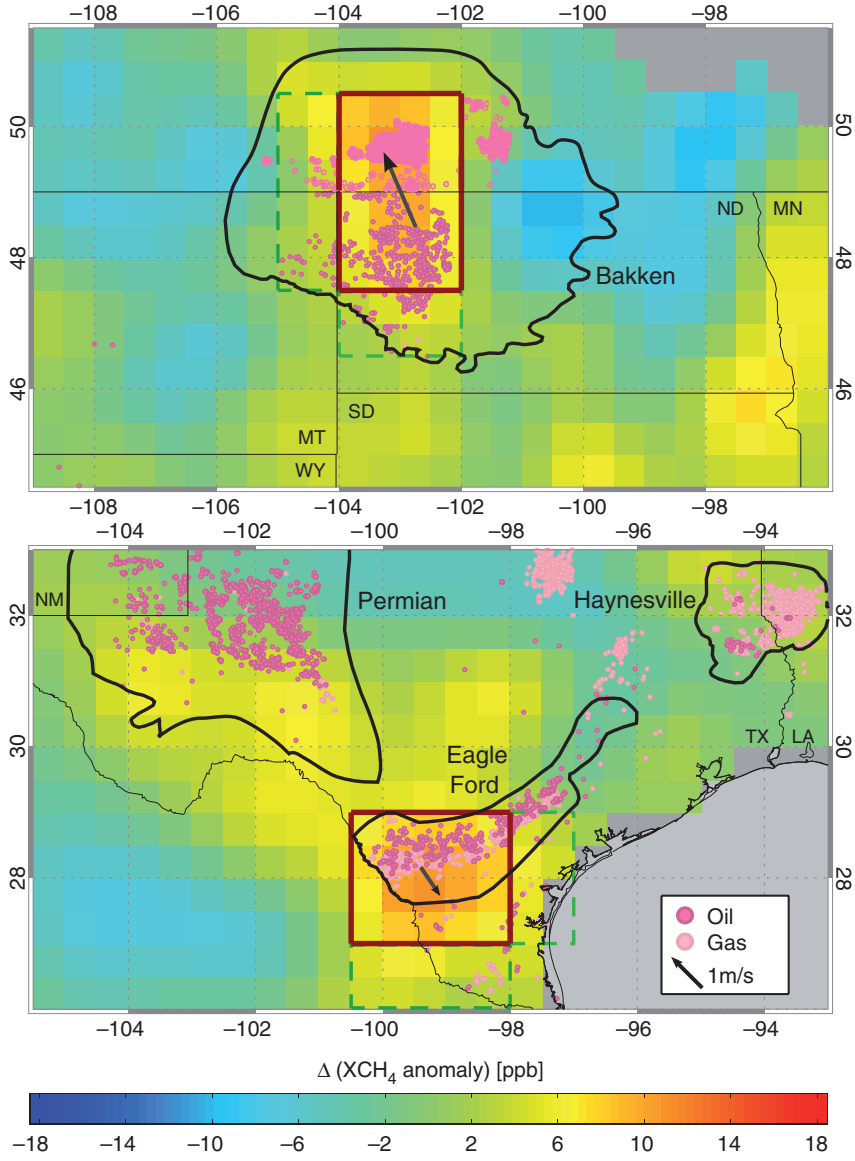

Figure 4. The difference between the mole fraction anomalies of methane, for the period 2009–2011 relative to the period 2006–2008. The locations of the oil and gas wells are shown in pink. The regions used for the box model estimates are red-rimmed. The corresponding regions used to determine the background values are framed by the green dashed lines. Averaged vectorial boundary layer wind differences between the periods are illustrated by dark grey arrows. Well positions are taken from the Fracking Chemical Database [*SkyTruth*, 2013] complemented by data for the Canadian part of the Bakken basin [*U.S. Energy Information Administration*, 2012].

where $l_{m(z)} = n_{m(z)} \Delta l_{m(z)}$ is the box dimension in meridional (zonal) direction, which is divided in $n_{m(z)}$ segments of the same length $\Delta l_{m(z)}$ (see Figure 6 for an illustration). The space-saving index notation $\cdot_{m(z)}$ means that there are two instances each, the meridional and the zonal one, e.g., $l_{m(z)} = n_{m(z)} \Delta l_{m(z)}$ means $l_m = n_m \Delta l_m$ and $l_z = n_z \Delta l_z$. The enhancement relative to the background upwind of the prevailing wind direction of the kth slice $E_{m(z),k}$ is computed from the averaged methane mole fractions XCH_4 and assumed O_2 columns (in units of molecules per area, estimated from the U.S. standard atmosphere and actual surface elevation) in the corresponding hot spot and background areas $A^h_{m(z),k}$ and $A^b_{m(z),k'}$

$$E_{m(z),k} = \frac{M_{CH_4} \cdot \left(XCH_4 \left(A^h_{m(z),k} \right) \cdot O_2 \left(A^h_{m(z),k} \right) - XCH_4 \left(A^b_{m(z),k} \right) \cdot O_2 \left(A^b_{m(z),k} \right) \right)}{N_A \cdot XO_2 \cdot AK} , \quad (2)$$

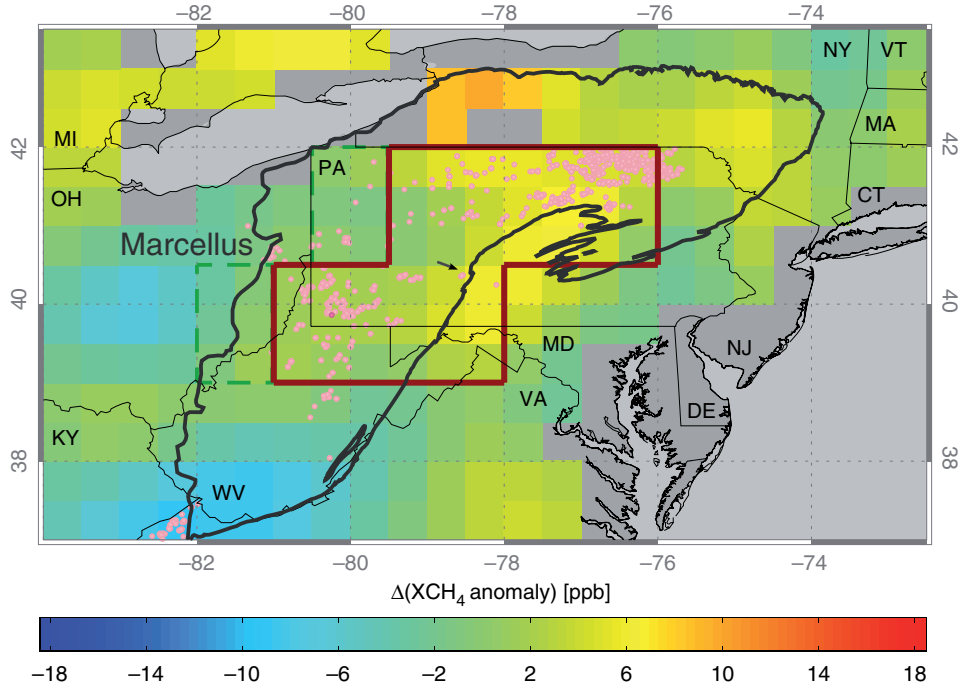

Figure 5. As Figure 4 but for the region containing the Marcellus shale formation.

where $M_{CH_4} = 16.04$ g/mol is the molar mass of methane, $N_A = 6.022 \cdot 10^{23}$ molec/mol is the Avogadro constant, $XO_2 = 0.209$ is the mixing ratio of oxygen in air, and AK is the dimensionless near-surface averaging kernel of the retrieval for appropriate conditions (Figure 1). Generally, k has a different range of values for $E_{m,k}$ and $E_{z,k}$ depending on the size of the hot spot area; there are n_m enhancements $\{E_{m,i}\}_{i=1}^{n_m}$ and n_z enhancements $\{E_{z,j}\}_{j=1}^{n_z}$. In the illustration shown in Figure 6, one has $n_m = 4$ and $n_z = 3$. According to Figure 4, one has $n_m = 6$ and $n_z = 4$ for Bakken as well as $n_m = 4$ and $n_z = 5$ for Eagle Ford.

Equation (1) is equivalent to

$$F = wEl\,;\; El := \frac{\overline{u}^2 E_m l_m + \overline{v}^2 E_z l_z}{\overline{u}^2 + \overline{v}^2}\,,\; w := \sqrt{\overline{u}^2 + \overline{v}^2}\,. \tag{3}$$

Hence, in the special cases $\overline{u} = \overline{v}$ or $E_m l_m = E_z l_z$ equation (1) simplifies to

$$F = \frac{w}{2}\left(E_m l_m + E_z l_z\right) \quad . \tag{4}$$

Since $\overline{u} \approx \overline{v}$ in the case of Bakken and $E_m l_m \approx E_z l_z$ in the case of Eagle Ford, equation (4) is a good approximation, which simplifies the error estimation. The uncertainty σ_F of F is computed via error propagation from the partial derivatives of F and the uncertainties of the individual contributing terms, σ_w, σ_{E_m}, and σ_{E_z}:

$$\begin{aligned}\sigma_F^2 &= \left(\frac{\partial F}{\partial w}\sigma_w\right)^2 + \left(\frac{\partial F}{\partial E_m}\sigma_{E_m}\right)^2 + \left(\frac{\partial F}{\partial E_z}\sigma_{E_z}\right)^2 \\ &= \frac{1}{4}\left(\left(E_m l_m + E_z l_z\right)^2 \sigma_w^2 + w^2\left(l_m^2\sigma_{E_m}^2 + l_z^2\sigma_{E_z}^2\right)\right).\end{aligned} \tag{5}$$

4. Results

The target regions containing the Bakken and Eagle Ford formations are shown in Figure 4. The differences between the mole fraction anomalies of atmospheric methane, for the period 2009–2011 relative to the period 2006–2008, clearly exhibit increases aligning with the analyzed oil and gas fields. The emission estimates are based on these anomaly differences and mean horizontal boundary layer wind. Vertical

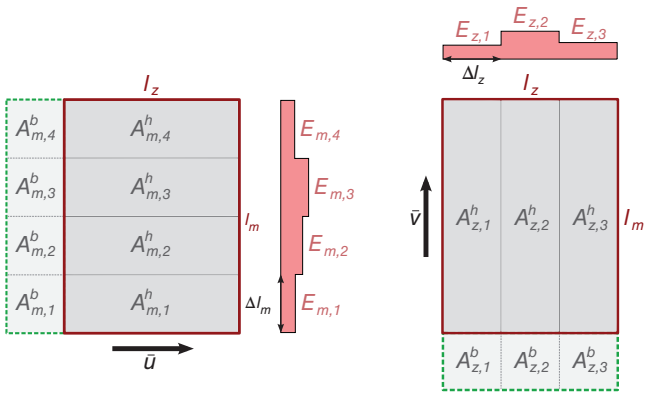

Figure 6. Illustration of the slicewise computation of $E_m l_m = \Delta l_m \sum_i E_{m,i}$ and $E_z l_z = \Delta l_z \sum_j E_{z,j}$ using the example of a 4×3 gridcell hot spot area. Notations are the same as used in the methods section of the manuscript. The background areas are chosen upwind of the prevailing direction of winds contributing to the averages $\bar{u}$ and $\bar{v}$.

transport can be approximately neglected, because the methane enhancements are derived for the whole column. The periods have been selected because drilling productivity in Bakken and Eagle Ford grew distinctly since 2009 [*U.S. Energy Information Administration*, 2014a]. We derive the following estimates for the emission increase between the selected periods using the mass-balance approach described in the methods section: 990 ± 650 $ktCH_4\ yr^{-1}$ and 530 ± 330 $ktCH_4\ yr^{-1}$ for the Bakken and Eagle Ford formation, respectively, corresponding to 1σ-uncertainty ranges of ±66% and ±62%.

The analogously obtained mole fraction anomaly differences for the target region containing the Marcellus shale formation are depicted in Figure 5. As in the case of Bakken and Eagle Ford, enhanced values occur in the vicinity of the production areas. However, the number of quality-filtered measurements per gridcell is smaller compared to the other two formations, and the resulting patterns are thus considered less reliable. This is a consequence of the location in mountainous terrain and the close proximity to the Great Lakes, which exhibit low surface reflectance. In combination with the large expanse of the Marcellus, extending throughout much of the Appalachians, and the more spacious distribution of wells, this hampers a straightforward definition of rectangular hot spot and adjacent background areas required for the introduced mass-balance approach. For these reasons, we refrain from estimating the Marcellus emission increase quantitatively in this way. However, the enhancement in the direction of the prevailing westerlies for the rectilinear polygonal region shown in Figure 5 would be consistent with a methane increase of about 17 $mgCH_4\ m^{-2}$, which is similar to the enhancements E_m and E_z obtained for Bakken and Eagle Ford.

The mean values and the uncertainties of the variable parameters E_m, E_z, and w for Bakken and Eagle Ford are summarized in Table 1. The uncertainties of E_m and E_z are derived from the spatial variability of methane inside the box and the background regions. The uncertainty of w accounts for temporal and spatial variability of wind inside the box, as well as differences in the mean meteorological conditions between the two considered periods. The main cause of the large uncertainties of the obtained mass flux estimates is the temporal averaging of winds over a long time span potentially including conditions that are not optimal for the mass-balance calculation applied here, e.g., stagnation and recirculation events, or gale. This complication will be overcome by future imaging satellite instruments with higher spatial resolution, temporal sampling, and better precision and thus dispensing with the need for long-time averaging. They will also facilitate a quantitative evaluation of emissions of the Marcellus shale formation. Additionally, future analysis will benefit from the usage of a three-dimensional (3-D) atmospheric transport model in the estimation of the fluxes.

Table 1. Summary of Variable Parameters Used to Calculate the Mass Fluxes of Methane F and Their Uncertainties

	Bakken		Eagle Ford	
Parameter	Mean Value	Variability (1σ)	Mean Value	Variability (1σ)
E_m	21.1 $mgCH_4\ m^{-2}$	11.0 $mgCH_4\ m^{-2}$	14.4 $mgCH_4\ m^{-2}$	7.4 $mgCH_4\ m^{-2}$
E_z	18.6 $mgCH_4\ m^{-2}$	7.2 $mgCH_4\ m^{-2}$	17.4 $mgCH_4\ m^{-2}$	7.7 $mgCH_4\ m^{-2}$
w	6.4 $m\ s^{-1}$	3.4 $m\ s^{-1}$	4.5 $m\ s^{-1}$	2.3 $m\ s^{-1}$
F	990 $ktCH_4\ yr^{-1}$	650 $ktCH_4\ yr^{-1}$	530 $ktCH_4\ yr^{-1}$	330 $ktCH_4\ yr^{-1}$

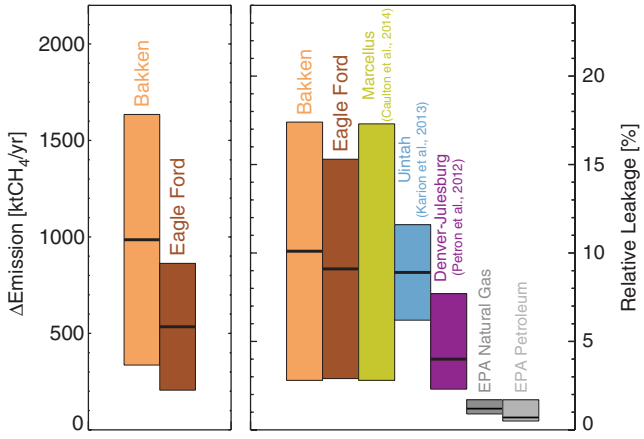

Figure 7. Estimated methane emissions are shown for the targeted regions Bakken in light brown, and Eagle Ford in dark brown. Shown are absolute emission increase (2009–2011 relative to 2006–2008) in the left panel, and the leakage rate relative to production in the right panel, in each case together with the 1σ-uncertainty ranges. For comparison, leakage estimates from previous studies in Marcellus (2012) [*Caulton et al.*, 2014], Uintah (2012) [*Karion et al.*, 2013], and Denver-Julesburg (2008) [*Pétron et al.*, 2012] (yellow, blue, and magenta) are shown together with the EPA bottom-up inventory estimates for natural gas and petroleum systems (2011) [*U.S. Environmental Protection Agency*, 2014] (grey) in the right panel.

The observed anomaly increment over Bakken, Eagle Ford, and Marcellus is attributed to increases of methane emissions, arising from the expanded hydraulic fracturing and increased oil and gas production over the intervening years, because the hot spot areas are broadly consistent with well positions and wind direction differences between both periods. Other potential anthropogenic emission sources, such as emissions from agriculture (e.g., enteric fermentation in livestock), were temporally constant to a first-order approximation [*U.S. Environmental Protection Agency*, 2013] and cancel out in the difference. Wetland emissions are assumed to vary only slightly between both periods, which is supported by inverse modeling results suggesting no increase in the Northern Hemispheric extra-tropics between the periods [*Bergamaschi et al.*, 2013]. Additionally, fluxes from wetlands are much smaller than anthropogenic sources in the United States [*Miller et al.*, 2013] and wetland extent does not match the observed enhancement patterns well, as concluded from the Kaplan wetland inventory [*Bergamaschi et al.*, 2007].

The production growth (sum of oil and gas) during the analyzed time periods (2009–2011 relative to 2006–2008) was about 250 kBOE/d (BOE = barrel of oil equivalent) for the Bakken [*Canadian National Energy Board*, 2011; *U.S. Energy Information Administration*, 2014a] and 150 kBOE/d for the Eagle Ford [*U.S. Energy Information Administration*, 2014a] formation. These values are based on gross production including not marketed natural gas. The emitted CH_4 mass estimated from the satellite data is converted to cubic feet natural gas by using the ideal gas law assuming standard conditions ($T = 288.15$ K, $p = 1013.25$ hPa) and a CH_4 content of 93% in natural gas [*U.S. Environmental Protection Agency*, 2013] with a realistic methane volume fraction range of 0.87–0.99 for high caloric gas. By converting the obtained emission estimate in cft/yr subsequently to kBOE/d, the following leakage-production ratios in terms of energy content result: 10.1% ± 7.3% for Bakken and 9.1% ± 6.2% for Eagle Ford. The estimated absolute emission increases and leakage rates relative to production for the analyzed formations are shown in Figure 7.

5. Discussion

The derived leakage ratios are considerably larger than the bottom-up estimates of 1.2% and 0.7% for natural gas and petroleum systems [*U.S. Environmental Protection Agency*, 2014]. Taking the associated uncertainties into account, methane emissions from energy production of both target formations are likely underestimated (88% probability) in current bottom-up inventories. The top-down leakage estimates for the two regions exceed the threshold value of 3.2% required for immediate climate benefit [*Alvarez et al.*, 2012]. This limit assumed switching from coal to natural gas for energy generation, but production in the analyzed formations is a mixture of gas and oil with Bakken being dominated by oil production. As oil produces more CO_2 per unit of energy than natural gas (140%) [*U.S. Energy Information Administration*, 2011], the threshold value must thus be further reduced and probably declines below the lower bound of the 1σ-uncertainty-range of the derived leakage ratio in both cases. In conclusion, at the current methane loss rates, a net climate benefit on all time frames owing to tapping unconventional resources in the analyzed tight formations is unlikely. Based on the derived leakage estimates, there does not seem to be any rationale to consider reinvigorating the share of petroleum in total electricity

generation of the United States, which has decreased to a modest value of 1% in recent years [*U.S. Energy Information Administration*, 2014b].

The top-down estimates presented are based on long-term satellite data and complement previous measurement-based results of other regions largely obtained during short-duration campaigns. Our leakage estimates are similar to the earlier results (Figure 7): 4.0% (2.3%–7.7%) for the Denver-Julesburg [*Pétron et al*., 2012], 8.9% (6.2%–11.7%) for the Uintah basin [*Karion et al*., 2013], and a possible range of 2.8%–17.3% for the Marcellus shale formation [*Caulton et al*., 2014]. On the other hand, it seems possible to reduce methane emissions by adopting new technology, as indicated by considerably lower leak rates close to the EPA inventory estimate found for selected production sites in the Gulf Coast, Midcontinent, Rocky Mountain, and Appalachian production regions of the United States [*Allen et al*., 2013]. This suggests that fugitive emissions vary widely from region to region depending on regulations and production practices.

In contrast to the methane leak rates reported in the literature, which are defined as total emissions divided by the total production, the leakages derived here are defined as the ratio of the emission increase between 2006–2008 and 2009–2011 divided by the production growth between these two periods. The direct comparison of the different rates thus inherently assumes that the added production between 2006–2008 and 2009–2011 leaks methane at the same rate as the total production. This is reasonable, because the industrial practices and thus the leak rates are considered to remain virtually constant between the periods in the analyzed regions. If the leakage in the later period had decreased relative to the former period, the rate based on the added production would be smaller than the total production leak rate.

The approach used in this study is optimal for regions such as Bakken, Eagle Ford, or Marcellus, where drilling productivity began to grow rapidly after 2009. However, it is not optimal to determine estimates for the Denver-Julesburg and Uintah basin for direct comparison, because it quantifies emission changes between two periods rather than total emissions. The production growth in those two basins is small for the chosen periods according to the Colorado Oil and Gas Conservation Commission (http://cogcc.state.co.us/) and the Division of Oil, Gas and Mining of the Utah Department of Natural Resources (http://oilgas.ogm.utah.gov/). Moreover, the rig count, which has for instance increased significantly in the Bakken, Eagle Ford, and Marcellus formations [*U.S. Energy Information Administration*, 2014a], has decreased in Colorado and Utah during the analyzed periods (2009–2011 relative to 2006–2008) [*Baker Hughes*, 2014]. As a consequence, a significant and large methane emission increase is not expected for the Denver-Julesburg and Uintah basin in the analyzed data set.

The above is also the most likely reason why the enhancement patterns over the Permian basin and gas-dense Haynesville region are less clear than those of the Bakken and Eagle Ford formations (Figure 4), despite prolific total production from these regions. The Permian basin is more mature than the younger plays, Bakken and Eagle Ford, with production and rig count virtually stagnating at high levels, whereas in Haynesville increasing production is concomitant with decreasing rig count, indicating increasing production efficiency with unknown impact on the emission trend [*U.S. Energy Information Administration*, 2014a]. One possible reason for this improved efficiency is that it pays off in the long run to invest in new technologies to reduce yield-decreasing fugitive emissions in natural gas systems, whereas in the tight oil production leakage of natural gas is typically not of primary interest in terms of profitability, because it is not the targeted resource itself and only used as an auxiliary agent to provide oil flow.

This is also reflected in the fact that a significant amount of the total natural gas extracted along with the oil in Bakken and Eagle Ford is flared or otherwise not marketed because the oil is considered more valuable or pipeline capacities and processing facilities to capture the gas are too costly. The waste of natural gas as a direct consequence of insufficient infrastructure is so extensive that both regions stand out clearly in satellite measurements of nighttime lights from the Visible Infrared Imaging Radiometer Suite (VIIRS) onboard the Suomi National Polar-orbiting Partnership (NPP) satellite [*Miller et al*., 2012].

In summary, SCIAMACHY nadir measurements show that anthropogenic CH_4 emissions from oil and gas production can be detected from space and that reported bottom-up leakage estimates are likely underestimated for specific formations. Further studies are needed to provide tighter constraints on fugitive

emissions and to investigate to what extent the high leakage rates obtained in this and other recent studies are representative for the entire North American oil and gas producing sector. Accurate evaluation of the impact and sustainability of unconventional oil and gas production across the globe is essential for the development of wise environmental and energy policy. Future wide swath imaging satellite instruments delivering higher spatial resolution, such as TROPOMI [*Veefkind et al*., 2012] and CarbonSat [*Bovensmann et al*., 2010; *Buchwitz et al*., 2013], a candidate for the eighth Earth Explorer of the European Space Agency (ESA), or the CarbonSat Constellation, when realized, will significantly enhance the current capabilities of satellite observations. CarbonSat and its constellation are projected to enable monitoring emissions down to the point-source scale [*Velazco et al*., 2011]. The better precision and accuracy of these new systems and concepts will yield time-resolved emission estimates during all stages of basin development to better identify the processes in the life cycle of oil and gas wells leading to the large methane emissions. Such future satellite missions, ideally supplemented by frequent aircraft and ground-based measurements, will provide independent verification of bottom-up inventories. This is essential for the reliable and accurate determination of the climate impact of exploiting unconventional energy resources in tight geologic formations.

Acknowledgments

The research leading to these results has in part been funded by the ESA project GHG-CCI, the DLR grant SADOS, the EU project ACCENT-Plus, and the University and the State of Bremen. Russell R. Dickerson was supported by NASA/AQAST. We thank ESA and DLR for providing the SCIAMACHY Level 1 data and the SCIAMACHY calibration team (DLR, SRON, University of Bremen, ESA, and others) for continuously improving the quality of the spectra. We acknowledge the use of data from the U.S. Energy Information Administration and the U.S. Environmental Protection Agency. We also thank the European Centre for Medium-Range Weather Forecasts (ECMWF) for providing the meteorological reanalysis data. Fracking well positions were obtained from SkyTruth via http://frack.skytruth.org/fracking-chemical-database/. North America rig counts were provided by Baker Hughes via http://phx.corporate-ir.net/phoenix.zhtml?c=79687&p=irol-reportsother. The methane data set used in this study is part of the second version of the Climate Research Data Package (CRDP#2) of the ESA project GHG-CCI and is available from http://www.esa-ghg-cci.org/.

References

Allen, D. T., et al. (2013), Measurements of methane emissions at natural gas production sites in the United States, *Proc. Natl. Acad. Sci. U. S. A.*, *110*(44), 17,768–17,773, doi:10.1073/pnas.1304880110.

Alvarez, R. A., S. W. Pacala, J. J. Winebrake, W. L. Chameides, and S. P. Hamburg (2012), Greater focus needed on methane leakage from natural gas infrastructure, *Proc. Natl. Acad. Sci. U. S. A.*, *109*(17), 6435–6440, doi:10.1073/pnas.1202407109.

Baker Hughes (2014), North America rig count. [Available at http://phx.corporate-ir.net/phoenix.zhtml?c=79687&p=irol-reportsother.]

Bergamaschi, P., et al. (2007), Satellite chartography of atmospheric methane from SCIAMACHY onboard ENVISAT: 2. Evaluation based on inverse model simulations, *J. Geophys. Res.*, *112*, D02304, doi:10.1029/2006JD007268.

Bergamaschi, P., et al. (2013), Atmospheric CH_4 in the first decade of the 21st century: Inverse modeling analysis using SCIAMACHY satellite retrievals and NOAA surface measurements, *J. Geophys. Res.*, *118*(13), 7350–7369, doi:10.1002/JGRD.50480.

Bovensmann, H., J. P. Burrows, M. Buchwitz, J. Frerick, S. Noël, V. V. Rozanov, K. V. Chance, and A. P. H. Goede (1999), SCIAMACHY—Mission objectives and measurement modes, *J. Atmos. Sci.*, *56*, 127–150, doi:10.1175/1520-0469(1999)056<0127:smoamm>2.0.co;2.

Bovensmann, H., M. Buchwitz, J. P. Burrows, M. Reuter, T. Krings, K. Gerilowski, O. Schneising, J. Heymann, A. Tretner, and J. Erzinger (2010), A remote sensing technique for global monitoring of power plant CO_2 emissions from space and related applications, *Atmos. Meas. Tech.*, *3*(4), 781–811, doi:10.5194/amt-3-781-2010.

Brandt, A. R., et al. (2014), Methane leaks from North American natural gas systems, *Science*, *343*(6172), 733–735, doi:10.1126/science.1247045.

Buchwitz, M., et al. (2013), Carbon monitoring satellite (CarbonSat): Assessment of atmospheric CO_2 and CH_4 retrieval errors by error parameterization, *Atmos. Meas. Tech.*, *6*(12), 3477–3500, doi:10.5194/amt-6-3477-2013.

Burrows, J. P., E. Hölzle, A. P. H. Goede, H. Visser, and W. Fricke (1995), SCIAMACHY—Scanning Imaging Absorption Spectrometer for Atmospheric Chartography, *Acta Astronaut.*, *35*(7), 445–451, doi:10.1016/0094-5765(94)00278-t.

Canadian National Energy Board (2011), Tight oil developments in the Western Canada sedimentary basin. [Available at http://www.neb-one.gc.ca/clf-nsi/archives/rnrgynfmtn/nrgyrprt/l/tghtdvlpmntwcsb2011/tghtdvlpmntwcsb2011-eng.pdf.]

Caulton, D. R., et al. (2014), Toward a better understanding and quantification of methane emissions from shale gas development, *Proc. Natl. Acad. Sci. U. S. A.*, *111*(17), 6237–6242, doi:10.1073/pnas.1316546111.

Dee, D. P., et al. (2011), The ERA-Interim reanalysis: Configuration and performance of the data assimilation system, *Q. J. R. Meteorol. Soc.*, *137*(656), 553–597, doi:10.1002/qj.828.

Dils, B., et al. (2014), The Greenhouse Gas Climate Change Initiative (GHG-CCI): Comparative validation of GHG-CCI SCIAMACHY/ENVISAT and TANSO-FTS/GOSAT CO_2 and CH_4 retrieval algorithm products with measurements from the TCCON, *Atmos. Meas. Tech.*, *7*(6), 1723–1744, doi:10.5194/amt-7-1723-2014.

Dlugokencky, E. J., et al. (2009), Observational constraints on recent increases in the atmospheric CH_4 burden, *Geophys. Res. Lett.*, *36*, L18803, doi:10.1029/2009GL039780.

Draxler, R. R., and G. D. Hess (2010), Description of the HYSPLIT_4 modeling system, *NOAA Tech. Memo. ERL ARL-224*, NOAA Air Resources Laboratory, Silver Spring, Md.

Howarth, R. W., R. Santoro, and A. Ingraffea (2011), Methane and the greenhouse-gas footprint of natural gas from shale formations, *Clim. Change*, *106*(4), 679–690, doi:10.1007/s10584-011-0061-5.

Intergovernmental Panel on Climate Change (2013), *Climate Change 2013: The Physical Science Basis. Contribution of Working Group I to the Fifth Assessment Report of the Intergovernmental Panel on Climate Change*, edited by T. F. Stocker, D. Qin, G.-K. Plattner, M. Tignor, S. K. Allen, J. Boschung, A. Nauels, Y. Xia, V. Bex, and P. M. Midgley, Cambridge Univ. Press, Cambridge, U. K.

Jackson, R. B., A. Down, N. G. Phillips, R. C. Ackley, C. W. Cook, D. L. Plata, and K. Zhao (2014), Natural gas pipeline leaks across Washington, DC, *Environ. Sci. Technol.*, *48*(3), 2051–2058, doi:10.1021/es404474x.

Karion, A., et al. (2013), Methane emissions estimate from airborne measurements over a western United States natural gas field, *Geophys. Res. Lett.*, *40*(16), 4393–4397, doi:10.1002/GRL.50811.

Kleipool, Q. L., R. T. Jongma, A. M. S. Gloudemans, H. Schrijver, G. F. Lichtenberg, R. M. van Hees, A. N. Maurellis, and R. W. M. Hoogeveen (2007), In-flight proton-induced radiation damage to SCIAMACHY's extended-wavelength InGaAs near-infrared detectors, *Infrared Phys. Technol.*, *50*(1), 30–37, doi:10.1016/j.infrared.2006.08.001.

Miller, S. D., S. P. Mills, C. D. Elvidge, D. T. Lindsey, T. F. Lee, and J. D. Hawkins (2012), Suomi satellite brings to light a unique frontier of nighttime environmental sensing capabilities, *Proc. Natl. Acad. Sci. U. S. A.*, *109*(39), 15,706–15,711, doi:10.1073/pnas.1207034109.

Miller, S. M., et al. (2013), Anthropogenic emissions of methane in the United States, *Proc. Natl. Acad. Sci. U. S. A.*, *110*(50), 20,018–20,022, doi:10.1073/pnas.1314392110.

Nisbet, E. G., E. J. Dlugokencky, and P. Bousquet (2014), Methane on the rise—Again, *Science*, *343*(6170), 493–495, doi:10.1126/science.1247828.
Pétron, G., et al. (2012), Hydrocarbon emissions characterization in the Colorado Front Range: A pilot study, *J. Geophys. Res.*, *117*(D4), D04304, doi:10.1029/2011JD016360.
Rigby, M., et al. (2008), Renewed growth of atmospheric methane, *Geophys. Res. Lett.*, *35*, L22805, doi:10.1029/2008GL036037.
Schneising, O., M. Buchwitz, M. Reuter, J. Heymann, H. Bovensmann, and J. P. Burrows (2011), Long-term analysis of carbon dioxide and methane column-averaged mole fractions retrieved from SCIAMACHY, *Atmos. Chem. Phys.*, *11*(6), 2863–2880, doi:10.5194/acp-11-2863-2011.
Schneising, O., et al. (2012), Atmospheric greenhouse gases retrieved from SCIAMACHY: Comparison to ground-based FTS measurements and model results, *Atmos. Chem. Phys.*, *12*(3), 1527–1540, doi:10.5194/acp-12-1527-2012.
Schneising, O., J. Heymann, M. Buchwitz, M. Reuter, H. Bovensmann, and J. P. Burrows (2013), Anthropogenic carbon dioxide source areas observed from space: Assessment of regional enhancements and trends, *Atmos. Chem. Phys.*, *13*(5), 2445–2454, doi:10.5194/acp-13-2445-2013.
SkyTruth (2013), SkyTruth fracking chemical database. [Available at http://frack.skytruth.org/fracking-chemical-database/frack-chemical-data-download.]
U.S. Energy Information Administration (2011), Voluntary reporting of greenhouse gases program, table of carbon dioxide emission factors for stationary combustion. [Available at http://www.eia.gov/oiaf/1605/coefficients.html.]
U.S. Energy Information Administration (2012), Shale oil maps. Bakken Shale Play, Williston Basin, North Dakota, Montana, Saskatchewan and Manitoba. [Available at http://www.eia.gov/oil_gas/rpd/shaleoil1.pdf.]
U.S. Energy Information Administration (2013), Technically recoverable shale oil and shale gas resources: An assessment of 137 shale formations in 41 countries outside the United States. [Available at http://www.eia.gov/analysis/studies/worldshalegas/pdf/overview.pdf.]
U.S. Energy Information Administration (2014a), Drilling productivity report, July 2014. [Available at http://www.eia.gov/petroleum/drilling/.]
U.S. Energy Information Administration (2014b), Monthly energy review, July 2014. [Available at http://www.eia.gov/totalenergy/data/monthly/pdf/mer.pdf.
U.S. Environmental Protection Agency (2012), Inventory of U.S. greenhouse gas emissions and sinks: 1990–2010. [Available at http://www.epa.gov/climatechange/Downloads/ghgemissions/US-GHG-Inventory-2012-Main-Text.pdf.]
U.S. Environmental Protection Agency (2013), Inventory of U.S. greenhouse gas emissions and sinks: 1990–2011. [Available at http://www.epa.gov/climatechange/Downloads/ghgemissions/US-GHG-Inventory-2013-Main-Text.pdf and http://www.epa.gov/climatechange/Downloads/ghgemissions/US-GHG-Inventory-2013-Annexes.pdf.]
U.S. Environmental Protection Agency (2014), Inventory of U.S. greenhouse gas emissions and sinks: 1990–2012. [Available at http://www.epa.gov/climatechange/Downloads/ghgemissions/US-GHG-Inventory-2014-Main-Text.pdf and http://www.epa.gov/climatechange/Downloads/ghgemissions/US-GHG-Inventory-2014-Annexes.pdf.]
Veefkind, J. P., et al. (2012), TROPOMI on the ESA Sentinel-5 precursor: A GMES mission for global observations of the atmospheric composition for climate, air quality and ozone layer applications, *Remote Sens. Environ.*, *120*, 70–83, doi:10.1016/j.rse.2011.09.027.
Velazco, V. A., M. Buchwitz, H. Bovensmann, M. Reuter, O. Schneising, J. Heymann, T. Krings, K. Gerilowski, and J. P. Burrows (2011), Towards space based verification of CO_2 emissions from strong localized sources: Fossil fuel power plant emissions as seen by a CarbonSat constellation, *Atmos. Meas. Tech.*, *4*(12), 2809–2822, doi:10.5194/amt-4-2809-2011.
Wunch, D., G. C. Toon, J.-F. L. Blavier, R. A. Washenfelder, J. Notholt, B. J. Connor, D. W. T. Griffith, V. Sherlock, and P. O. Wennberg (2011), The total carbon column observing network, *Philos. Trans. R. Soc. A*, *369*, 2087–2112, doi:10.1098/rsta.2010.0240.